

Carbonic Anhydrase-Related Protein VIII Deficiency Is Associated With a Distinctive Lifelong Gait Disorder in Waddles Mice

Yan Jiao,* Jian Yan,[†] Yu Zhao,[‡] Leah Rae Donahue,[§] Wesley G. Beamer,[§] Xinmin Li,**
Bruce A. Roe,^{††} Mark S. LeDoux[‡] and Weikuan Gu*¹

*Departments of Orthopedic Surgery-Campbell Clinic and Pathology, University of Tennessee Health Science Center, Memphis, Tennessee 38163, [†]Department of Biology, University of Memphis, Memphis, Tennessee 38163, [‡]Departments of Neurology and Anatomy and Neurobiology, University of Tennessee Health Science Center, Memphis, Tennessee 38163, [§]The Jackson Laboratory, Bar Harbor, Maine 04609, **Functional Genomics Facility, University of Chicago, Chicago, Illinois 60637 and ^{††}Department of Chemistry and Biochemistry, University of Oklahoma, Norman, Oklahoma 73019

Manuscript received April 14, 2005
Accepted for publication July 29, 2005

ABSTRACT

The waddles (*wdl*) mouse is a unique animal model that exhibits ataxia and appendicular dystonia without pathological abnormalities of either the central or the peripheral nervous systems. A 19-bp deletion in exon 8 of the carbonic anhydrase-related protein VIII gene (*Car8*) was detected by high-throughput temperature-gradient capillary electrophoresis heteroduplex analysis of PCR amplicons of genes and ESTs within the *wdl* locus on mouse chromosome 4. Although regarded as a member of the carbonic anhydrase gene family, the encoded protein (CAR8) has no reported enzymatic activity. In normal mice, CAR8 is abundantly expressed in cerebellar Purkinje cells as well as in several other cell groups. Compatible with nonsense-mediated decay of mutant transcripts, CAR8 is virtually absent in mice homozygous for the *wdl* mutation. These data indicate that the *wdl* mouse is a *Car8* null mutant and that CAR8 plays a central role in motor control.

RODENTS, mainly spontaneously mutant mice with movement disorders, have revealed molecules and cellular pathways involved in motor control. Examples of deficient or defective proteins in mice with motor dysfunction include *Scn8a* (type VIII α -subunit of voltage-gated sodium channel) in *Med^J* mice (BURGESS *et al.* 1995), *Grid2* (delta2 glutamate receptor) in lurcher mice (ZUO *et al.* 1997), *Kcnj6* (potassium inwardly rectifying channel subfamily J member 6) in weaver mice (PATIL *et al.* 1995), *Agtppb1* (ATP/GTP-binding protein 1) in Purkinje cell degeneration mice (FERNANDEZ-GONZALEZ *et al.* 2002), and *Cacna1a* (P/Q type calcium channel α -1A subunit) in tottering mice (FLETCHER *et al.* 1996). Although these models have shed considerable light on signaling and second messenger pathways, the relationship between cellular dysfunction due to these mutations and motor control at the systems level remains unclear. This disconnect is largely due to the ubiquitous expression of the encoded proteins within neural tissues. Furthermore, many mutant rodents with movement disorders exhibit overt structural and histological abnormalities of the central nervous system, extraneural disease, or early death. Thus, in many cases, the mutant gene may

have deleterious effects on several local-area neural networks in addition to systemic effects that severely compromise attempts to correlate genotype with particular motor phenotypes (*e.g.*, ataxia, Parkinsonism, dystonia, spasticity, or myoclonus). Identification of additional mutant genes with restricted expression in neural tissue and causally associated with distinct motor syndromes may help to bridge the gaps between the molecular and systems neurobiology of movement disorders. As part of this effort, we chose to study waddles (*wdl*) mice.

The *wdl* mutation was discovered at The Jackson Laboratory (TJL) in 1995 in C57BL/KS mice (<http://www.jax.org/mmr/waddler.html>). The *wdl* phenotype is very similar to that of another model, waddler (*wd*), which was discovered in 1959 and is now thought to be extinct (YOON 1959). The gait of *wdl* mice is characterized by wobbly side-to-side ataxic movements that are readily seen when mice reach 2 weeks of age. The gait disorder of *wdl* mice persists throughout their life span.

In addition to ataxia, *wdl* mice exhibit frequent tail elevation and intermittent Straub tail. During ambulation, the trunks of *wdl* mice are abnormally elevated, particularly their caudal portions. Resting forelimb and hindlimb tone is normal. However, action dystonia with apparent cocontraction of knee and elbow flexors and extensors is exacerbated by ambulation (JINNAH and

¹Corresponding author: University of Tennessee Health Science Center, A331 Coleman Bldg., 956 Court Ave., Memphis, TN 38163.
E-mail: wgu@utmem.edu

HESS 2004). This appendicular dystonia produces nearly straight limbs with minimal flexion at the knee and elbow joints, elevation of the pelvis, and a “bouncy” or “waddling” motion during ambulation, particularly at higher velocities. Occasionally, *wdl* mice fall to their sides.

Pathological examination of *wdl* mice at TJL was unremarkable except for one isolated case of hydrocephalus. In addition, vision and hearing were normal in the mutants. An early genetic study indicated that *wdl* mice were autosomal recessive mutants. Linkage mapping at TJL placed the *wdl* mutation in close approximation to the *wd* locus on mouse chromosome 4, although tests for allelism were not conducted since *wd* is extinct.

MATERIALS AND METHODS

Mice: One homozygous waddles (*wdl/wdl*) mouse and its heterozygous littermate (+/*wdl*) from (L.R.D.) mouse mutant stock resource colonies at TJL were sent to (W.G.) University of Tennessee Health Science Center (UTHSC). Then a breeding colony was established by mating them at UTHSC. Experimental animal procedures and mouse husbandry were performed in accordance with the National Institute of Health's *Guide for the Care and Use of Laboratory Animals* and approved by the UTHSC Institutional Animal Care and Use Committee.

Motor function examination: Adult (2–4 months) *wdl/wdl* mice and wild-type (+/+) littermates were used for quantitative analyses of motor function. The open field behavior of additional *wdl* mice along with heterozygote (+/*wdl*) and +/+ littermates was observed in both home cages and bedless arenas. Digital videos were analyzed for the presence of distinguishing behaviors. Analysis of variance was conducted for the significance between the homozygous *wdl* (*wdl/wdl*) and their normal littermates (+/*wdl* or +/+) whenever necessary.

Rotarod: Mice were acclimated to a rotarod (San Diego Instruments) rotating at 5 rpm for 5 min prior to data acquisition. Three 2-min trials were performed at each target speed (5, 10, 20, 30, 40, and 50 rpm) with an intertrial interval of 5 min. The rotarod was accelerated to target speeds >1 min. Median values were used for statistical comparisons.

Footprint analysis: Mouse forepaws and hindpaws were dipped in nontoxic water-based paints. Mice were then allowed to run down a runway lined with white paper. Three trials were performed with intertrial intervals of at least 5 min. Two to four steps from the middle portion of each run were measured for (1) stride length, (2) hind-base width (the distance between the right and left hindlimb strides), (3) front-base width (the distance between the right and left forelimb strides), and (4) overlap between forepaw and hindpaw placement. At least seven steps were measured for each mouse. Mean values were used for statistical analyses.

Tail suspension: This test involved the response of each mouse to 1 min of suspension from the tail. Some mice with neurological dysfunction exhibited hindlimb and/or forelimb clasping during this maneuver.

Righting reflex: To obtain righting reflex times, mice were placed in the supine position and then released. The time required for all four limbs to contact the tabletop was measured for three trials. Median values were used for statistical comparisons.

Vertical rope climbing: Mice were acclimated to a vertical 40-cm-long, 10-mm-thick rope prior to testing. The bottom of

the rope was suspended 15 cm above a padded base and the top entered an escape box. Three trials with a 5-min intertrial interval were completed for each mouse and median times were used for statistical analyses.

Raised-beam task: Mice were acclimated to an 80-cm-long, 26-mm-wide beam elevated 50 cm above a padded foundation. A 60-W lamp at the start served as an aversive stimulus whereas the opposite end of the beam entered an escape box. Slips were counted as mice traversed the beam. Falls were counted as five slips.

Genome information: Information on microsatellite markers and their locations were obtained from the Mouse Genome Database search forms (<http://www.informatics.jax.org/searches/markerform.shtml>). The locations of microsatellite markers on genome sequences and physical chromosomal distances were obtained by searching the Ensembl mouse genome database (http://www.ensembl.org/Mus_musculus); data used in this article are from its updated information as of March 20, 2005.

High-throughput screening of the *wdl* locus: Liver genomic DNA (gDNA) from +/+, +/*wdl*, and homozygous (*wdl/wdl*) mice was extracted for temperature-gradient capillary electrophoresis (TGCE) and sequence analysis. On the basis of the Ensembl and National Center for Biotechnology Information (NCBI) databases, primer pairs flanking the exons of known and predicted genes (including ESTs) within the *wdl* locus were designed with Primer3 software (http://www-genome.wi.mit.edu/cgi-bin/primer/primer3_www.cgi). Primers were located ~100 bp 5' or 3' to each exon and, in general, produced 300- to 400-bp DNA fragments. Several primer pairs were required for complete coverage of some exons. PCR amplification of gDNA was performed in a 96-well plate format and consisted of 30–35 cycles at three temperatures: strand denaturation at 96° for 30 sec, primer annealing at 54°–60° for 60 sec, and primer extension at 72° for 120 sec. TGCE (SpectruMedix, State College, PA) was used to analyze amplicons from +/+, +/*wdl*, and *wdl/wdl* mice mixtures. The SpectruMedix system includes a high-throughput capillary electrophoresis instrument capable of analyzing 96 samples every 140 min. Heteroduplex analysis was subsequently performed offline using SpectruMedix software. Amplicons from *wdl* mice were sequenced if they differed from normal.

RT-PCR: Total RNA was extracted from cerebellum and liver with Trizol reagent (Invitrogen, San Diego). Total RNA integrity was confirmed with the Agilent Bioanalyzer 2100. Reverse transcription and PCR were conducted using a one-step RT-PCR kit from Invitrogen. Reactions were performed in a total volume of 50 μ l with 8 ng/ μ l of total RNA and 0.2 μ M forward (CCAAAACAATTCCATGCTTTAAT) and reverse (GTATGAATTCCAGAAGCTGTGGT) primers used to amplify exons 6–9 of *Car8*. First, cDNA synthesis and pre-denaturation were performed in single cycles at 50° for 40 min and 94° for 2 min. Next, PCR amplification was performed for 35 cycles: 94° for 30 sec, 54°–58° for 36 sec, and 72° for 2 min.

DNA sequencing: DNA sequencing was conducted to verify the deletion in the gDNA and cDNA of *Car8*. PCR products from both genomic and cDNA were purified using an AMPure PCR Purification Kit (Agencourt Beverly, MA) and the purified products were sequenced using a BigDye Terminator v3.1 Cycle Sequencing (Applied Biosystems, Foster City, CA). A total of 5- μ l sequencing reactions, including 2- μ l of Big Dye (plus Half-BD), 10–23 ng of purified DNA template, and 1–3 pmol of either forward or reverse universal sequencing primers, were incubated for 37 cycles at 96° for 180 sec, 50° for 30 sec, and 60° for 180 sec. Unreacted primers were removed by ethanol-acetate precipitation (3.75% 3 M NaOAc, 87.5% nondenatured 100% EtOH, and 8.75% dH₂O, pH 4.6). The labeled products were dissolved in 0.02 mM EDTA in HiDi

formamide prior to electrophoretically loading onto the SpectruMedix 96 capillary sequencing system. The same primers in the amplification of DNA fragments from either genomic DNA or mRNA were also used in the sequencing. Sequencing was conducted two times to verify the result for either gDNA or cDNA.

Expression of recombinant CAR8: Normal (accession no. NM_007592) and mutant *Car8* cDNA was amplified (forward primer, CACCATGGCTGACCTGAGCTTCATTG; reverse primer, CTGAAAGGCCGCTCGGATGACTCTAT) and cloned into Invitrogen's pET102/D-TOPO vector in-frame for transcription. A single colony of *Escherichia coli* BL21 (DE3) transformed with the *Car8* expression vector was inoculated into 10 ml of Luria-Bertani medium containing 100 µg/ml ampicillin; this was incubated at 37° for 10 hr. Then 0.5 ml of the culture was inoculated into 50 ml of Luria-Bertani medium containing 100 µg/ml ampicillin. This culture was incubated at 37° until it reached an OD₆₀₀ of 0.7. At that point, isopropyl-D-thiogalactoside was added to a final concentration of 0.5 mM and incubation was continued at 37° for 3 hr; cells were harvested by centrifugation. Protein products were analyzed on 8% SDS-PAGE gels. Calculated molecular weights for normal and mutant CAR8 fusion proteins are 46.09 and 45.49 kD, respectively.

Northern blot hybridization: After isolation of total RNA from mouse cerebella, mRNA (from 20 mice: +/+, 7; *wdl/wdl*, 7; +/*wdl*, 6) was extracted and purified with the Micro-Poly(A)Purist kit from Ambion (Austin, TX). The mRNA was electrophoretically resolved on denaturing gels and transferred to positively charged nylon membranes. Radiolabeled ([³²P]UTP) complementary RNA (cRNA) probes were generated by *in vitro* transcription using T7 RNA polymerase. The location of *Car8* probe in the cDNA of Car 8 gene is from 205 to 650 bp. After ultraviolet crosslinking, blots were prehybridized and then hybridized overnight with both *Car8* and β-actin cRNA probes. After washing, blots were exposed to Kodak Biomax MR radiographic film prior to development.

Antibody production: A rabbit polyclonal antibody to CAR8 was generated by immunizing rabbits with a peptide sequence unique to CAR8 (DANGEYQSPINLSREC) and encoded by nucleotides 27–71 from the second exon of *Car8* (AnaSpec, San Jose, CA). This peptide shows no sequence similarity with other carbonic anhydrases. Serum was immunoaffinity purified.

Western blot analysis: Cerebellar cortex was harvested from mice, rinsed in PBS, and homogenized in chilled NP-40 lysis buffer containing a protease inhibitor cocktail (Sigma, St. Louis). Lysates were clarified by centrifugation. Protein concentrations were determined with the Bio-Rad (Hercules, CA) DC protein assay kit using BSA standards. Equal amounts of proteins were electrophoretically resolved on 4–20% Tris-HCl Criterion precast gels (Bio-Rad) and then transferred onto Immunoblot PVDF membranes (Bio-Rad). Membranes were washed in Tris-buffered saline with 0.1% Tween, blocked in 5% nonfat dry milk, and then incubated in affinity-purified rabbit anti-CAR8 (1:2000) or rabbit anti-inositol 1,4,5-triphosphate receptor (IP₃R1) (1:2000, A. G. Scientific, San Diego) antibodies. After washing, blots were incubated in horseradish-peroxidase-conjugated secondary antibodies (1:5000, Amersham, Buckinghamshire, UK). Targeted proteins were visualized with the ECL Plus chemiluminescent kit from Amersham. For loading controls, membranes were stripped and reprobed with a mouse anti-β-tubulin antibody (1:5000; Chemicon, Temecula, CA).

Immunocytochemistry: Mice and rhesus monkeys were perfusion fixed with saline/4% paraformaldehyde. Brains were postfixed and then cryoprotected in 30% sucrose/phosphate buffer. Mouse brains and monkey cerebella were sectioned parasagittally on a cryostat and collected onto Superfrost-Plus glass slides (Fisher). Mouse spinal cords were sectioned horizontally. Brain sections were processed for immunocyto-

chemical detection of CAR8 (affinity-purified rabbit antibody, 1:20,000), calbindin (rabbit polyclonal antibody, 1:5000; Chemicon), and IP₃R1 (rabbit polyclonal antibody, 1:2000). For light microscopic visualization, tissues were sequentially exposed to a biotinylated goat anti-rabbit polyclonal antibody (1:500; Vector, Burlingame, CA), streptavidin, and diaminobenzidine. Cy2- and rhodamine red-X-conjugated (Jackson ImmunoResearch, West Grove, PA) secondary antibodies were applied for confocal microscopy.

RESULTS

Motor dysfunction in *wdl* mice: To characterize the motor function of *wdl* mice, several experiments were performed to compare the mutants with +/+ littermates. There were no differences between *wdl* and +/+ mice in their responses to tail suspension. Furthermore, righting times and vertical rope climbing, respectively, did not differ between the mutants and their normal littermates, suggesting that the *wdl* mice have normal axial and appendicular motor power. In contrast, the results of footprint analysis (Figure 1, A and B), rotarod (Figure 1C), and the raised-beam task were compatible with significant motor disability in *wdl* mice. Although traversal times on the raised-beam task did not differ significantly between *wdl* mice and +/+ littermates, the mutants had many more slips (19.0 ± 1.7) than normal (0.8 ± 0.3) littermates ($P < 0.0001$). In *wdl* mice, paws were abnormally everted and hindpaw (red) placement was rostral to the location of forepaw (green) prints (Figure 1A). However, there were no differences in either stride length or the distance of paw overlap between *wdl* and +/+ mice (Figure 1B). At all speeds, *wdl* mice showed shorter latencies to fall off the rotarod than +/+ littermates ($P < 0.05$, for all).

High-throughput screening of the *wdl* locus on chromosome 4: According to data from the Jackson Laboratory web page (http://www.informatics.jax.org/menu/marker_menu.shtml), the recombination estimates with standard errors and the best gene order were: centromere—D4Mit149 1.79 ± 1.02 cM—*wdl*— 0.81 ± 0.80 cM (D4Mit181, D4Mit99)— 7.65 ± 4.16 cM—D4Mit97— 2.52 ± 2.47 cM—D4Mit39— 1.62 ± 1.60 cM—D4Mit5. To begin with, we searched the Ensembl database (http://www.ensembl.org/Mus_musculus) to locate genetic markers flanking the *wdl* locus. Initially, *D4mit149* (at 0 cM), the nearest marker on the centromeric side of the *wdl* locus, was mapped between 3,584,271 and 3,584,381 bp. *D4mit181* (at 2.5 cM), the nearest marker on the telomeric side, was mapped between 9,500,798 and 9,500,930 bp (Figure 2A). Another marker on the telomeric side, *D4mit99*, was mapped between 12,496,147 and 12,496,289 bp. However, the initial mapping data from TJL were based on 86 F₂ mice. By examining the genomic information, we found that the region from centromere to 12,500,000 bp is a gene-poor region with 68 genes and 41 ESTs, mainly from the region between 6,500,000 and 12,500,000 bp (Figure 2A). Those genetic

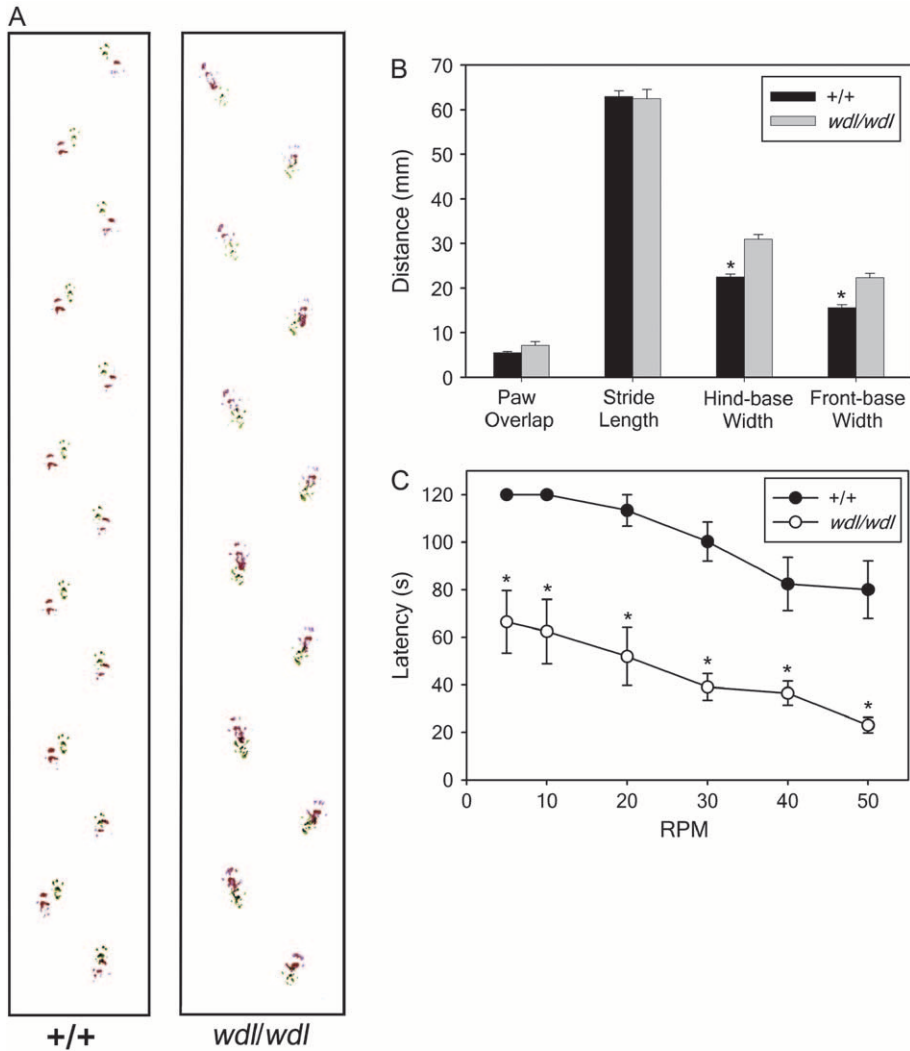


FIGURE 1.—Behavioral analysis of *wdl* mice and *+/+* littermates. (A) Representative footprint patterns from *+/+* and *wdl/wdl* mice. (B) Quantitative footprint analysis. (C) Latency to fall off the rotarod plotted *vs.* speed in revolutions per minute (rpm). (* $P < 0.05$). The error bar denotes standard deviation.

elements were then analyzed with TGCE. Every exon and at least 50 bp of intron sequences on both sides from *wdl* and normal mice were amplified and carefully compared on the SpectruMedix system. During this screening process, we found that only the *Car8* exon 8 amplicon was smaller in *wdl* mice than in *+/+* littermates (forward primer, AATTGTCTCCCAAATCC ATC; reverse primer, CAGCATGCTTTCTTAACCACTG) (Figure 2B). Every DNA fragment from other genes was the same between *wdl* and its *+/+* littermates. After verification of this difference by PCR amplification of *Car8* exon 8 (Figure 2C), we conducted a comparison of PCR products from eight mouse strains and *wdl/wdl* mice (Figure 2D), and the data indicated that the deletion found in *wdl* mice did not exist in any of these normal mouse strains (Figure 2E). At that point, we felt confident that a deletion within exon 8 of *Car8* caused the *wdl* disease. We then sequenced exon 8 and discovered that 19 nucleotides were deleted in the mutant mice (Figure 2F).

***Car8* mutation:** *Car8* has nine exons (ENSMUSG 00000041261). Total RNA from normal and *wdl* mice

was extracted for RT-PCR amplification of 3' *Car8* transcript (exons 6–9) (Figure 3A). Smaller amplicons were found in cerebella (Figure 3A) and extraneural tissue (liver, lung, and kidney) from *wdl* mice (data not shown). Direct sequencing of *Car8* cDNA from normal and *wdl* mice confirmed the 19-nucleotide deletion (Figure 3B). In the region of deletion, 15 nucleotides are flanked by two AAGG motifs. The deleted 19 nucleotides include the 15 nucleotides and one AAGG motif, leaving the other AAGG motif in the genome. Thus, the deletion either starts at the first AAGG motif and stops at the second AAGG motif or starts immediately after the first AAGG motif and stops after the second motif. Due to frameshifting, *wdl Car8* cDNA is predicted to encode a protein that is 29 amino acids shorter than *+/+* CAR8 secondary to elimination of 50 *+/+* amino acids and addition of 21 novel residues before terminating in a stop codon (Figure 3B).

***Car8* transcript and protein (CAR8):** To determine the molecular impact of the *Car8* deletion mutation, we compared mutant and *+/+* *Car8* at the transcriptional and translational levels. Six bands were identified on

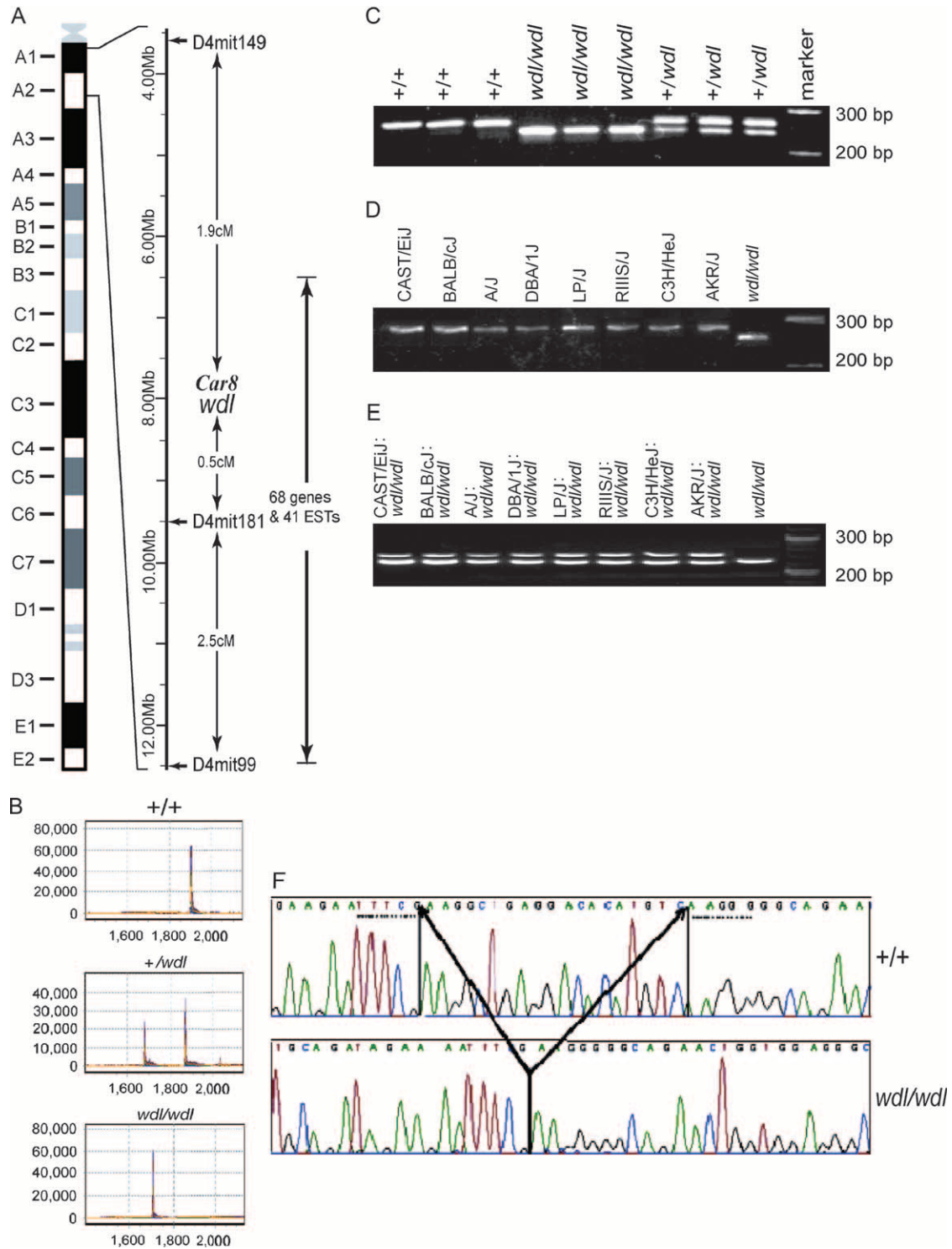


FIGURE 2.—A genomic map of the *wdl* locus (A) shows the relative locations of microsatellite markers. TGCE detected an abnormality in exon 8 of the *Car8* gene (B). PCR amplification of *Car8* exon 8 generated a smaller band in *wdl/wdl* mice, a larger band in *+/+* mice, and two bands in *+/wdl* mice (C). Comparison of PCR products from eight mouse strains and *wdl/wdl* mice (D) revealed that the deletion does not exist in any normal mouse strains (E). DNA sequence analysis revealed a 19-bp deletion in *Car8* exon 8 from *wdl/wdl* mice (F).

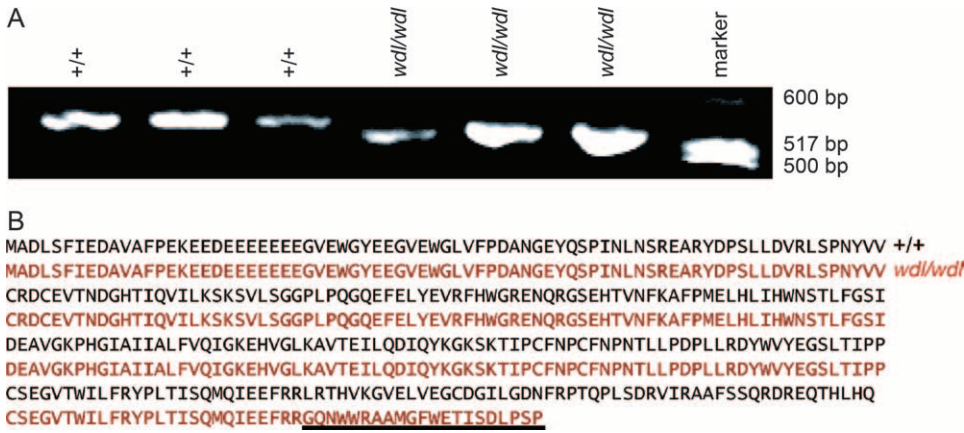


FIGURE 3.—Analysis of *Car8* transcript with RT-PCR. (A) Amplification of *Car8* transcript from total RNA extracted from cerebella of +/+ and *wdl/wdl* mice. (B) Derived amino acid sequences of normal (black) and mutant CAR8 (brown).

Northern blotting of mRNA from both +/+ and *wdl* mice (Figure 4A). However, a striking global reduction of *Car8* transcript was detected in *wdl* mice (Figure 4A). The larger bands on the Northern blot were barely detectable in the mutants. Quantities of *Car8* mRNA were intermediate in +/*wdl* animals. With Western blotting, our affinity-purified rabbit polyclonal antibody to CAR8 identified both full-length recombinant +/+ and *wdl* CAR8 in different sizes (Figure 4B). In contrast, we were unable to detect CAR8 in cerebellar tissue lysates from *wdl* mice although a Purkinje cell marker, the type 1 IP₃R1, was expressed at normal levels in the mutants (Figure 4C).

Immunolocalization of CAR8: Immunohistochemistry was then used to examine the patterns of CAR8 expression in +/+ and *wdl* mice (Figure 5). In +/+ mice, CAR8 was expressed in cerebellar Purkinje cells as well as in cerebellar nuclei and brainstem (Figure 5A). Immunohistochemically, CAR8 expression was greatest in cerebellar Purkinje cells and minimal to absent in the spinal cord and cerebral cortex. In line with the Western blotting results, CAR8 expression was virtually undetectable in *wdl* mice (Figure 5B). The potential importance of CAR8 to humans is suggested by its prominent ex-

pression in Purkinje cells from a nonhuman primate (Figure 5C). CAR8 is abundantly present in the somas, axons, and entire dendritic arbors of cerebellar Purkinje cells (Figure 5, D and E). The common Purkinje cell marker, calbindin, showed immunoreactivity in cerebellar cortex that did not differ between normal and mutant mice (Figure 5, F and G). Furthermore, at the level of confocal microscopy, the density and intracellular localization of IP₃R1 was normal in *wdl* mice (Figure 5, H and I).

DISCUSSION

Our data strongly suggest that the 19-bp deletion in *Car8* described here is causally associated with the *wdl* phenotype. We provide several lines of evidence to support this claim. First, *Car8* is located within the genetic region of the *wdl* locus. Second, the *Car8* deletion was the only defect detected among genes and ESTs within the *wdl* locus from *wdl* mice. Because the *wdl* mutation was derived from the C57BLKS inbred strain and there are no other differences between *wdl* mice and their littermates, it is unlikely that another mutation causes

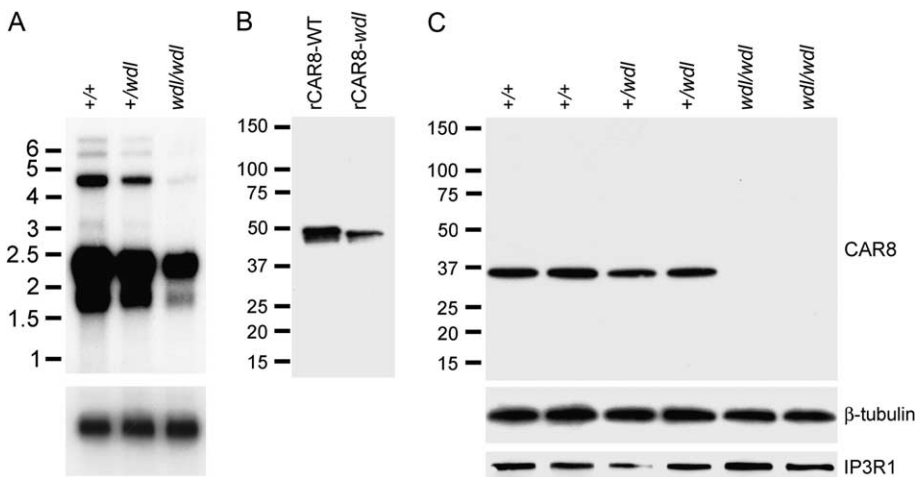


FIGURE 4.—The *wdl Car8* mutation has dramatic effects at the transcriptional and translational levels. (A) Northern blot analysis of cerebellar mRNA. (B) Western blot analysis of recombinant wild-type (rCAR8-WT) and mutant (rCAR8-*wdl*) proteins. (C) Western blot analysis of cerebellar lysates from +/+, +/*wdl*, and *wdl/wdl* mice; β-tubulin was the loading control.

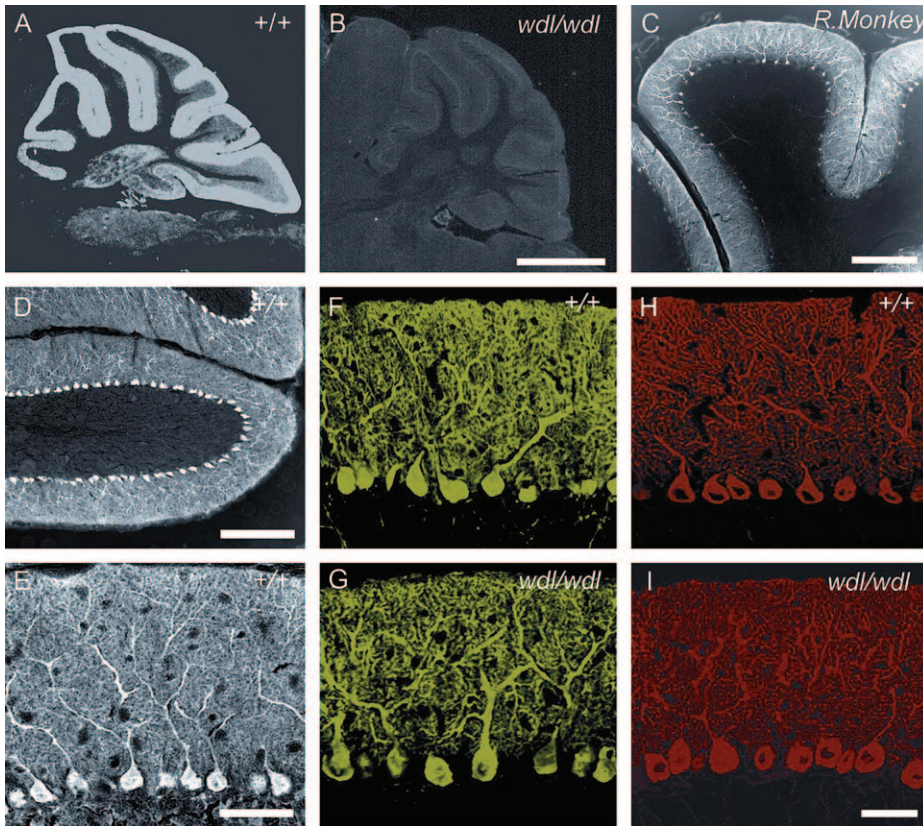


FIGURE 5.—Immunocytochemistry for CAR8 and Purkinje cell markers in +/+ and *wdl/wdl* mice and a rhesus monkey (R.Monkey). CAR8 in the cerebellum from +/+ (A, D, and E) and *wdl/wdl* (B) mice and a rhesus monkey (C). Also shown is calbindin (F and G) and IP₃R1 (H, I) expression in +/+ (F and H) and *wdl/wdl* (G and I) mice. Bars: A and B, 1 mm; C, 500 μm; D, 100 μm; E–I, 50 μm.

the movement disorder exhibited by *wdl* mice. Third, work on the cDNA sequence agreed with the genomic data. Finally, we showed a virtual absence of CAR8 expression in *wdl* mice but not in wild-type littermates.

Our molecular analysis of the *wdl* mouse model has shown that CAR8 is essential for motor control. Moreover, the relative preponderance of CAR8 in cerebellar Purkinje cells suggests that the *wdl* mouse can be used as a tool to precisely investigate the effects of Purkinje cell dysfunction on local and wide-area motor networks. In contrast to several other mouse mutants with ataxia, there is no loss or overt morphological abnormalities of Purkinje cells in *wdl* mice. Although CAR8 is a member of the carbonic anhydrase family of zinc metalloenzymes that catalyze the reversible hydration of CO₂, CAR8 lacks catalytic activity by virtue of missing critical amino acid residues required for zinc binding (SJOBLÖM *et al.* 1996; TANIUCHI *et al.* 2002). Recombinant CAR8 generated by introducing R117H and E115Q mutations into the wild-type protein is able to bind zinc and catalyze the hydration of CO₂. CAR8 may contribute to the pathophysiology of ataxia in other mouse models. For instance, KELLY *et al.* (1994) reported the absence of *Car8* transcript in the cerebella of lurching mice years before the actual causal mutation was identified.

The reduced *Car8* transcript and barely detectable CAR8 protein in *wdl* mice is indicative of nonsense-mediated decay (NMD). NMD, first documented by

LOSSON and LACROUTE (1979) >20 years ago, is a proof-reading mechanism that enables eukaryotic cells to detect and degrade mRNAs that contain premature termination codons (PTCs). About one-third of inherited genetic disorders and many forms of cancer are caused by frameshift or nonsense mutations, which result in the generation of PTCs (FRISCHMEYER and DIETZ 1999; HOLBROOK *et al.* 2004). Although mRNA containing a PTC may initially be translated into a truncated protein, cells can initiate the NMD mechanism to recognize and degrade the mutant transcripts if the truncated protein is deleterious (WAGNER and LYKKE-ANDERSEN 2002).

With respect to the cellular effects of CAR8 deficiency, it has been shown that CAR8 binds to the modulatory domain of IP₃R1, which is an intracellular IP₃-gated Ca²⁺ channel (HIROTA *et al.* 2003). CAR8 inhibits IP₃ binding to IP₃R1 by reducing the affinity of the receptor for IP₃ (HIROTA *et al.* 2003). IP₃ is an intracellular second messenger for calcium release. Increased cytosolic-free calcium concentration is a stimulatory signal for diverse calcium-dependent mechanisms such as secretion, contraction, or alterations in membrane excitability. Therefore, CAR8 deficiency may cause ataxia by altering calcium homeostasis and disturbing the normal physiology of cerebellar Purkinje cells.

Our study also demonstrates a useful strategy for simplifying positional cloning. Most procedures employed

in traditional positional cloning have been labor intensive and time consuming. As described in MATERIALS AND METHODS, our strategy includes identifying a target genomic region on the basis of linkage mapping, identifying every gene and biologically functional element within the candidate region, TGCE heteroduplex analysis (CHOU *et al.* 2005; GIRALD-ROSA *et al.* 2005), confirmation of suspected mutations by cDNA sequencing, and, finally, investigation of the encoded protein. Using a similar approach, we recently identified the causal mutation in a mouse disease model of spontaneous fractures (JIAO *et al.* 2005). In that study, mapping of the mutation locus was followed by positional cloning. In this study, mapping information on the TJL webpage allowed us to define a target genomic region. The mutant gene was discovered in less than half a year from the start of the project, thereby offering the possibility of rapid identification of mutations with only crude mapping data. We believe that our strategy will be particularly useful for familial human diseases with small kindreds. Furthermore, in the setting of rodent models with spontaneous mutations, mutations can be rapidly identified without the excessive cost and time associated with the extensive breeding programs required for high-resolution mapping.

In summary, we have identified a 19-bp deletion in exon 8 of *Car8* in *wdl* mice using a positional candidate cloning approach. This loss-of-function mutation of *Car8* may underlie the ataxic phenotype of *wdl* mice. Since we did not find an obvious change in the morphology of Purkinje cells or the distribution of the CAR8-binding target, IP₃R1, the cellular pathways by which CAR8 deficiency causes ataxia and dystonia remain uncertain. Thus, the role of CAR8 cerebellar neurophysiology warrants additional study.

Special recognition and gratitude are offered to Belinda Harris of The Mouse Mutant Resource at The Jackson Laboratory for providing mice and to Feng Jiao of the University of Tennessee Health Science Center for mouse breeding, tissue collection, and management of this work. Major support for this work was provided by the Center of Genomics and Bioinformatics (W.G.) and the Center in Connective Tissue Research (W.G.), at University of Tennessee Health Science Center. Additional support was from the Dystonia Medical Research Foundation (M.S.L.), the Veterans Administration at Memphis Medical Center (W.G.), National Institute of Arthritis and Musculoskeletal and Skin Diseases, National Institutes of Health (NIH; R01 AR51190 to W.G.; RR01183 to L.R.D.); National Eye Institute, NIH (R01 EY12232 to M.S.L.; R01 EYO15073 to L.R.D.); National Institute of Neurological Diseases and Stroke, NIH (R01 NS048458 to M.S.L.).

LITERATURE CITED

- BURGESS, D. L., D. C. KOHRMAN, J. GALT, N. W. PLUMMER, J. M. JONES *et al.*, 1995 Mutation of a new sodium-channel gene, *Scn8a*, in the mouse mutant 'motor endplate disease.' *Nat. Genet.* **10**: 461–465.
- CHOU, L. S., F. GEDGE and E. LYON, 2005 Complete gene scanning by temperature gradient capillary electrophoresis using the cystic fibrosis transmembrane conductance regulator gene as a model. *J. Mol. Diagn.* **7** (1): 111–120.
- FERNANDEZ-GONZALEZ, A., A. R. LA SPADA, J. TREADAWAY, J. C. HIGDON, B. S. HARRIS *et al.*, 2002 Purkinje cell degeneration (*pcd*) phenotypes caused by mutations in the axotomy-induced gene, *Nna1*. *Science* **295**: 1904–1906.
- FLETCHER, C. F., C. M. LUTZ, T. N. O'SULLIVAN, J. D. SHAUGHNESSY, JR., R. HAWKES *et al.*, 1996 Absence epilepsy in tottering mutant mice is associated with calcium channel defects. *Cell* **87**: 607–617.
- FUREMAN, B. E., H. A. JINNAH and E. J. HESS, 2002 Triggers of paroxysmal dyskinesia in the calcium channel mouse mutant tottering. *Pharmacol. Biochem. Behav.* **73**: 631–637.
- GIRALD-ROSA W., R. A. VLEUGELS, A. C. MUSIEK and J. E. SLIGH, 2005 High-throughput mitochondrial genome screening method for nonmelanoma skin cancer using multiplexed temperature gradient capillary electrophoresis. *Clin. Chem.* **51** (2): 305–11.
- HIROTA, J., H. ANDO, K. HAMADA and K. MIKOSHIBA, 2003 Carbonic anhydrase-related protein is a novel binding protein for inositol 1,4,5-trisphosphate receptor type 1. *Biochem. J.* **372**: 435–441.
- HOLBROOK, J. A., G. NEU-YILIK, M. W. HENTZE and A. E. KULOZIK, 2004 Nonsense-mediated decay approaches the clinic. *Nat. Genet.* **36**: 801–808.
- JIAO, Y., X. LI, W. G. BEAMER, J. YAN, Y. TONG *et al.*, 2005 A deletion causing spontaneous fracture identified from a candidate region of mouse chromosome 14. *Mamm. Genome* **16**: 20–31.
- JINNAH, H. A., and E. J. HESS, 2004 *Animal Models of Movement Disorders*, pp. 55–72, edited by M. S. LEDOUX. Elsevier, San Diego.
- KELLY, C., A. NOGRADI, R. WALKER, K. CADDY, J. PETERS *et al.*, 1994 Lurching, reeling, waddling and staggering in mice—Is carbonic anhydrase (CA) VIII a candidate gene? *Biochem. Soc. Trans.* **22**: 359S.
- LOSSON, R., and F. LACROUTE, 1979 Interference of nonsense mutations with eukaryotic messenger RNA stability. *Proc. Natl. Acad. Sci. USA* **76**: 5134–5137.
- PATIL, N., D. R. COX, D. BHAT, M. FAHAM, R. M. MYERS *et al.*, 1995 A potassium channel mutation in weaver mice implicates membrane excitability in granule cell differentiation. *Nat. Genet.* **11**: 126–129.
- SJOBLOM, B., B. ELLEBY, K. WALLGREN, B. H. JONSSON and S. LINDSKOG, 1996 Two point mutations convert a catalytically inactive carbonic anhydrase-related protein (CARP) to an active enzyme. *FEBS Lett.* **398**: 322–325.
- TANIUCHI, K., I. NISHIMORI, T. TAKEUCHI, Y. OHTSUKI and S. ONISHI, 2002 cDNA cloning and developmental expression of murine carbonic anhydrase-related proteins VIII, X, and XI. *Brain Res. Mol. Brain Res.* **109**: 207–215.
- WAGNER, E., and J. LYKKE-ANDERSEN, 2002 mRNA surveillance: the perfect persist. *J. Cell Sci.* **115**: 3033–3038.
- YOON, C. H., 1959 Waddler, a new mutation, and its interaction with quivering. *J. Hered.* **50**: 238–244.
- ZUO, J., P. L. DE JAGER, K. A. TAKAHASHI, W. JIANG, D. J. LINDEN *et al.*, 1997 Neurodegeneration in Lurcher mice caused by mutation in delta2 glutamate receptor gene. *Nature* **388**: 769–773.

Communicating editor: M. JUSTICE